Electronic Supplementary Information:

Influence of the Glycocalyx on the Size and Mechanical Properties of Plasma Membrane-Derived Vesicles

Purvil Jani[a], Marshall J. Colville[a,b], Sangwoo Park[a,b], Youlim Ha[a], Matthew J. Paszek*[a,b,c] and Nicholas L. Abbott*[a]

[a]*Robert Frederick Smith School of Chemical and Biomolecular Engineering, Cornell University, Ithaca, NY 14853, USA*
[b]*Field of Biophysics, Cornell University, Ithaca, NY 14853, USA*
[c]*Nancy E. and Peter C. Meining School of Biomedical Engineering, Cornell University, Ithaca, NY 14853, USA*
** Corresponding author. Email: mpj31@cornell.edu (Matthew J. Paszek), nabbott@cornell.edu (Nicholas L. Abbott)*

1. Non-uniform coverage of Muc1 on GPMVs

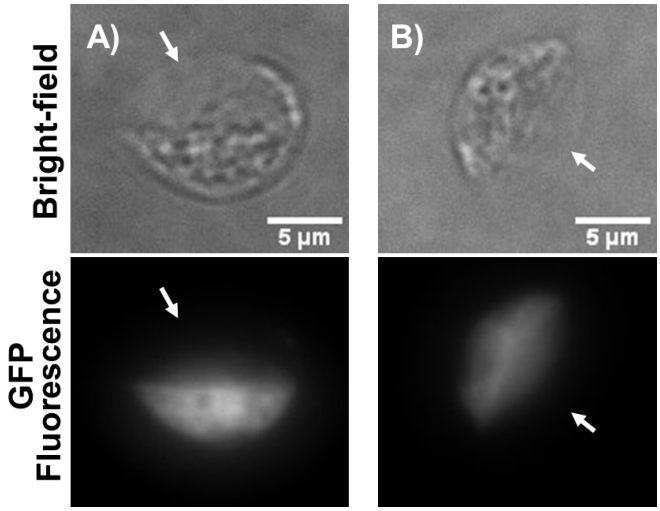

Fig. S1 (A and B) Bright-field and fluorescence micrographs of GPMVs strained in nematic DSCG (13.8 wt%) showing a non-uniform coverage of Muc1 on their membranes.

2. Straining cells in nematic DSCG

We studied the mechanical properties of 1E7 cells by dispersing them in an osmotically balanced aqueous solution of DSCG [1] (final DSCG concentration of 13.8 wt%, nematic phase) and compared cell shapes to control MCF10A cells (wild type cells). As shown in Fig. S2A and C, we observed that both 1E7 and wild type cells are strained weakly and remain nearly spherical in nematic DSCG. LC elastic stresses have been previously observed to strain synthetic GUVs in a size-dependent manner such that the extent of straining of GUVs decreases with increase in size (Eq. 7) (GUVs of surface area > 500 µm^2 were observed to be strained weakly) [2]. Previously, we have shown that human red blood cells (RBCs) can be strained to a significant extent (R/r = 1.5-3) by dispersing them in nematic DSCG solutions that are osmotically balanced with the RBC interior [1]. Because the sizes of epithelial cells used in this study (~15-20 µm) are larger than RBCs (~ 7-8 µm), the surface energy ($E_S \propto R^2$) dominates the LC elastic energy ($E_{LC} \propto R$) resulting in weak straining of 1E7 and wild type cells.

Moreover, cellular organelles and the cytoskeleton of epithelial cells resist strain by LC elastic forces, increasing the apparent cell rigidity [3].

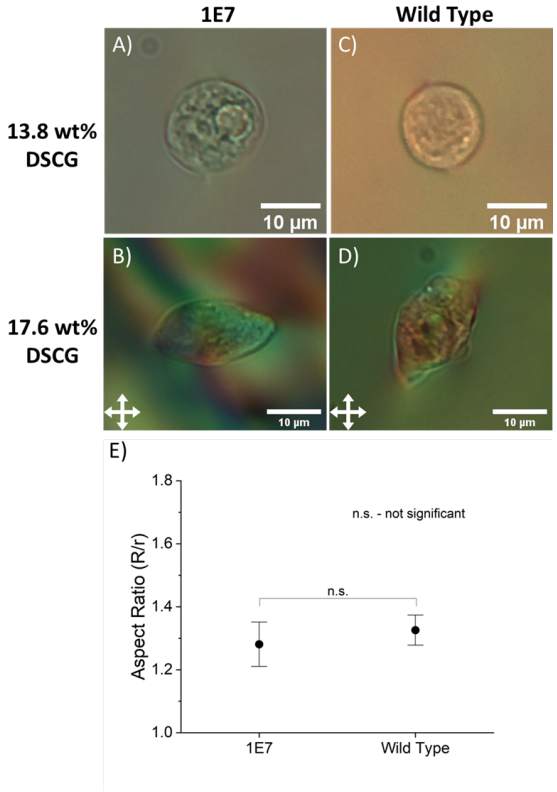

Fig. S2 (A, B) Optical micrographs (bright-field and crossed polars, respectively) of 1E7 cells in 13.8wt% DSCG (R/r = 1.87) and in 17.6wt% DSCG (R/r = 1.65), respectively. (C, D) Optical micrographs (bright-field and crossed polars, respectively) of wild-type cells in 13.8wt% DSCG and in 17.6wt% DSCG, respectively. (E) Distribution of aspect ratios of 1E7 and wild type cells dispersed in 17.6wt% DSCG.

The elastic constants of nematic DSCG increase with an increase in concentration of DSCG. Moreover, a hypertonic solution dehydrates cells, which allows them to be strained to high aspect ratios. As shown in Fig. S2B and D, we observed that it is possible to strain 1E7 and wild type cells by dispersing them in solutions with high DSCG concentrations (17.6 wt%) which is a hypertonic solution for the cells.

3. LC director profile around GPMVs

We quantified the orientation of the LC around GPMVs by using a Polscope. For this experiment, we imaged GPMVs using an Olympus BX60 microscope (Olympus Life Science) equipped with a PolaViz Phi-Viz polarized imaging system (Model P391, PolaViz). The images of GPMVs were captured and analyzed using a PolaViz imaging software (Version 3, PolaViz) to obtain a map of the LC director profile. As shown in Fig. S3, we observed that the director profile of the LC around 1E7 GPMVs is consistent with a weak tangential anchoring of the LC on the GPMV membrane. Moreover, we

observed the treatment of 1E7 GPMVs with StcE mucinase had no measurable influence on the anchoring of the LC on their membranes.

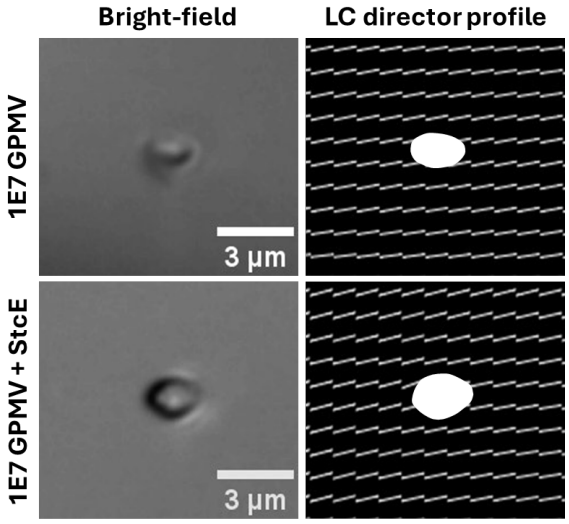

Fig. S3 Bright-field micrographs and Polscope maps of LC director profile around 1E7 GPMV and 1E7 GPMV + StcE (white ellipsoidal masks in maps of LC director profile indicate the locations of GPMVs).

4. Evaluation of $\frac{\partial E_{LC}}{\partial\left(\frac{R}{r}\right)}$, $\frac{\partial E_S}{\partial\left(\frac{R}{r}\right)}$ and $\frac{\partial E_B}{\partial\left(\frac{R}{r}\right)}$

To probe the influence of various energies on the shapes of GUVs in LCs, we evaluated the rate of change of E_{LC}, E_S, and E_B with respect to the GUV aspect ratio (i.e., $\frac{R}{r}$). Using Eq. 1-6, the three energies can be expressed as,

$$E_{LC} = CK\left(\frac{3V}{4\pi}\right)^{\frac{1}{3}}\left(\frac{R}{r}\right)^{-\frac{4}{3}} \tag{8}$$

$$E_S = 2\tau\pi\left(\frac{\left(\frac{R}{r}\right)asin\left(\left(1-\frac{1}{\left(\frac{R}{r}\right)^2}\right)^{\frac{1}{2}}\right)}{\left(1-\frac{1}{\left(\frac{R}{r}\right)^2}\right)^{\frac{1}{2}}}+1\right)\left(\frac{3V}{4\pi\left(\frac{R}{r}\right)}\right)^{\frac{2}{3}} \tag{9}$$

$$E_B = \frac{2778046668940015\,\kappa\left(\frac{3}{8\left(\frac{R}{r}\right)^2} + \frac{\left(\left(\frac{R}{r}\right)^2\left(\frac{3V}{4\left(\frac{R}{r}\right)\pi}\right)^{\frac{1}{3}}\right)}{\left(\frac{R}{r}\right)\left(\frac{3V}{4\left(\frac{R}{r}\right)\pi}\right)^{\frac{1}{3}} + \left(\frac{3V}{4\left(\frac{R}{r}\right)\pi}\right)^{\frac{1}{3}}} + \frac{9}{8}\right)}{281474976710656} + \frac{2778046668940015\left(\frac{R}{r}\right)C_0^2\kappa\left(\frac{3V}{4\left(\frac{R}{r}\right)\pi}\right)^{\frac{2}{3}}}{562949953421312} - 4C_0\kappa\pi\epsilon'\left(\left(\frac{R}{r}\right)^2\right)\left(\frac{3V}{4\left(\frac{R}{r}\right)\pi}\right)^{\frac{1}{3}} \quad (10)$$

where ϵ' is the complementary complete elliptic integral of the second kind [4]. We then evaluated the rate of change of the three energies with respect to the GUV aspect ratio ($\frac{R}{r}$), at a constant GUV volume (V), using the *diff()* function in MATLAB (MATLAB R2023b). For $\frac{R}{r} = 1.3$, $V = 500$ μm^3, $\kappa = 10^{-19}$ J, $\tau = 5 \times 10^{-6}$ N/m, $C = 6$, and $C_0 = 0$, we calculate $\frac{\partial E_B}{\partial\left(\frac{R}{r}\right)} \sim 5 \times 10^{-19}$ J to be negligible in comparison to $\frac{\partial E_{LC}}{\partial\left(\frac{R}{r}\right)} \sim -2 \times 10^{-16}$ J and $\frac{\partial E_S}{\partial\left(\frac{R}{r}\right)} \sim 1 \times 10^{-16}$ J. Moreover, our calculations reveal that this conclusion holds for values of $\frac{R}{r}$ from 1.05 to 4 and for V from 5 μm^3 to 5000 μm^3. This result indicates that the spindle-like shapes assumed by the GUVs in the LC are not influenced by E_B.

5. Quantitative fluorescence microscopy

We tested whether the trend of increasing GFP fluorescence intensity per area with GPMV surface area shown in Fig. 4A is an artifact of microscopy. To this end, we prepared giant unilamellar vesicles (GUVs) consisting of 99 mol% of synthetic phospholipid DOPC and 1 mol% of 1,2-dioleoyl-sn-glycero-3-phosphoethanolamine-N-(lissamine rhodamine B sulfonyl) (ammonium salt) by the method of electroformation described previously [5]. We found that the fluorescence intensity per area of GUVs increased with their surface areas (fluorescence intensity per area ∝ (GUV Surface area)$^{0.09}$) (Fig. S4A). Hence, as shown in Fig. S4B, to compensate for this area dependence of fluorescence intensity we normalized the measured fluorescence intensity of GUVs as

$$Normalized\ fluorescence\ intensity\ per\ area = \frac{(Measured\ fluorescence\ intensity\ per\ area)}{(Surface\ area\ of\ GUV)^{0.09}}$$

Moreover, upon performing this normalization for 1E7 GPMV data shown in Fig. 4A, we found that normalized GFP fluorescence intensity per area increased significantly as the surface area of GPMVs increased (Fig. S4C).

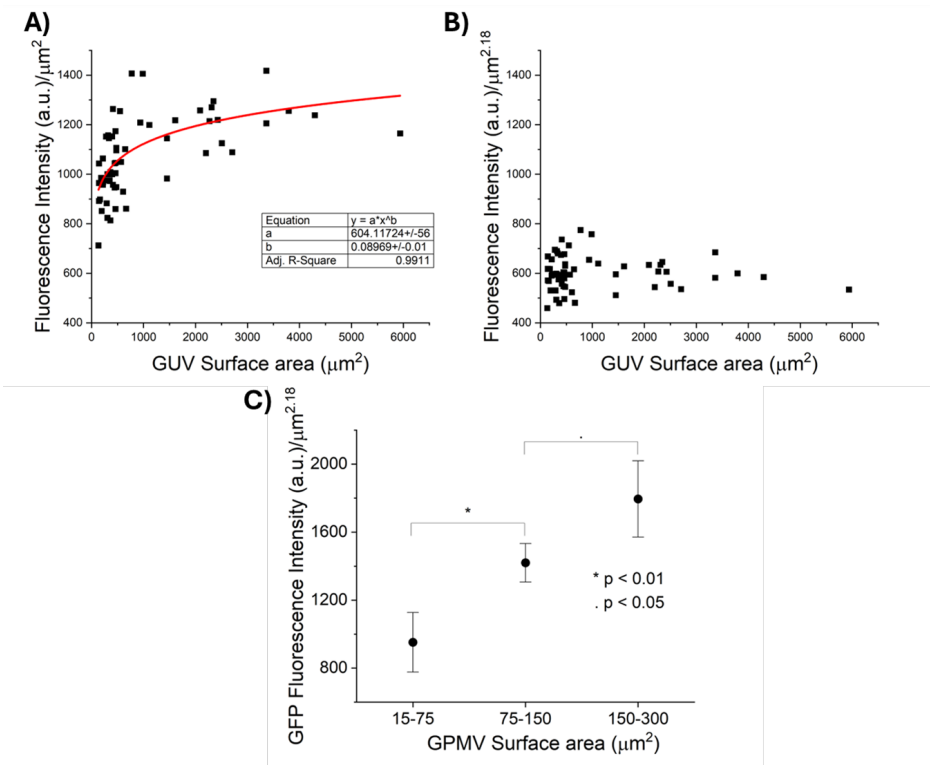

Fig. S4 (A, B) Plot of raw and normalized values of fluorescence intensity per unit area of GUVs as a function of their surface areas, respectively. (C) Plot of normalized GFP fluorescence intensity per unit area of GPMVs of 3 different surface area ranges (data represent mean ± standard error).

6. Influence of bending modulus

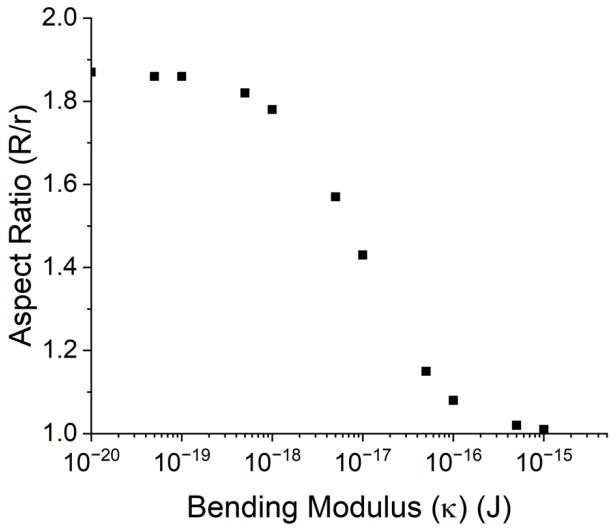

Fig. S5 Plot of predicted values of aspect ratios of GPMVs as a function of their membrane bending modulus (κ)

7. Spontaneous curvature of GPMVs

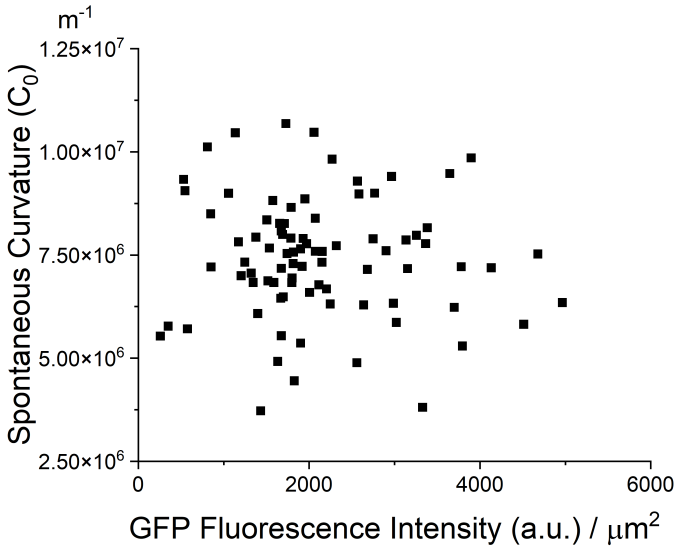

Fig. S6 Plot of calculated values of spontaneous curvature of GPMVs as a function of GFP fluorescence intensity

8. Absence of tubules on GPMVs

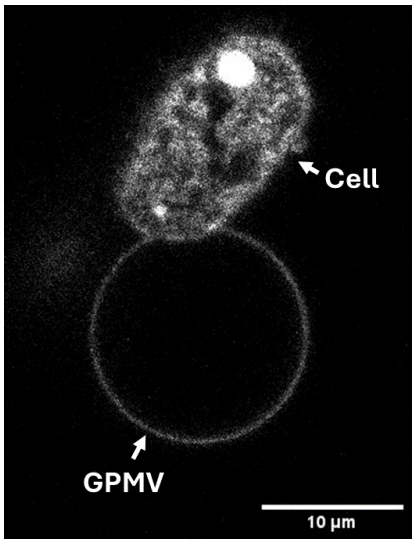

Fig. S7 Confocal micrograph (GFP signal) of a 1E7 cell and a GPMV blebbing from it.

9. GPMVs with R/r < 1.54

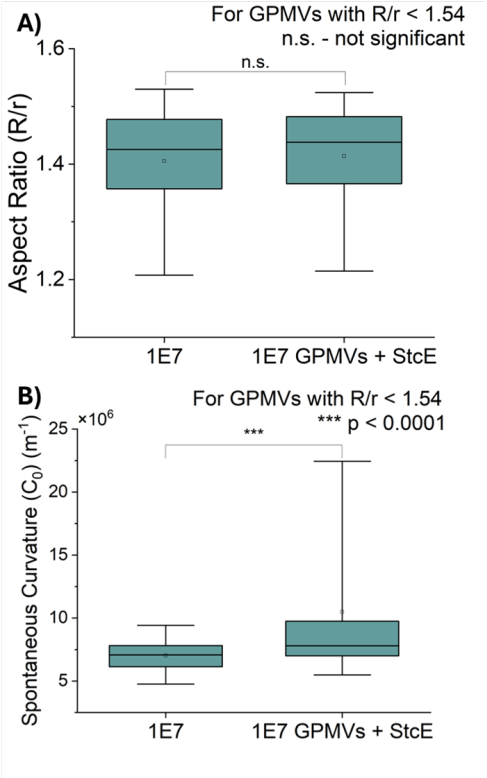

Fig. S8 Plots of (A) aspect ratios and (B) spontaneous curvature of 1E7 GPMVs and 1E7 GPMVs treated with StcE mucinase for GPMVs with aspect ratio < 1.54.

References

1. K. Nayani, A. A. Evans, S. E. Spagnolie and N. L. Abbott, *Proc Natl Acad Sci U S A*, 2020, **117**, 26083-26090.
2. P. C. Mushenheim, J. S. Pendery, D. B. Weibel, S. E. Spagnolie and N. L. Abbott, *Proc Natl Acad Sci U S A*, 2016, **113**, 5564-5569.
3. D. A. Fletcher and R. D. Mullins, *Nature*, 2010, **463**, 485-492.
4. E. T. Whittaker and G. N. Watson, *A Course in Modern Analysis*, Cambridge University Press, Cambridge, England, 4th edn., 1996.
5. P. Jani, K. Nayani and N. L. Abbott, *Soft Matter*, 2021, **17**, 9078-9086.